Synthesis, Electronic Structure, Molecular Packing/Morphology Evolution, and Carrier Mobilities of Pure Oligo-/Poly(alkylthiophenes)

Lei Zhang,[†] Nicholas S. Colella,[†] Feng Liu,[†] Stephan Trahan,[†] Jayanta K. Baral,[†] H. Henning Winter,[‡] Stefan C. B. Mannsfeld,[§] and Alejandro L. Briseno*,[†]

[†]Department of Polymer Science and Engineering, Conte Research Center and [‡]Department of Chemical Engineering, University of Massachusetts, Amherst, Massachusetts 01003, United States

[§]Stanford Synchrotron Radiation Lightsource, Menlo Park, California 94025, United States

S *Supporting Information*

ABSTRACT: Monodispersed conjugated oligothiophenes are receiving attention in fundamental and applied science due to their interesting optical, optoelectronic, and charge transport properties. These "low molecular weight" polymers serve as model structures for the corresponding polymer analogues, which are inherently polydispersed. Here we report the synthesis, electronic structure, molecular packing/morphology, and charge transport properties of monodispersed oligothiophenes with up to six didodecylquaterthiophene (DDQT) building block repeat units (i.e., 24 thiophene units). At the point where the effective conjugation length is reached, the electronic structure showed convergence behavior to the corresponding polymer, poly(3,3″-didodecyl-quaterthiophene) (PQT-12). X-ray crystal structure analysis of the dimer (DDQT-2) showed that terminal thiophenes exhibit *syn*-conformations, similar to the terminal *syn*-conformations observed in the trimer (DDQT-3). The dimer also exhibits a rare bending of the terminal alkyl side chains in order to prevent steric hindrance with neighboring hydrogens attached to core thiophenes. Grazing incidence X-ray scattering measurements revealed a morphology evolution from small molecule-like packing to polymer-like packing in thin films, with a morphology transition occurring near the effective conjugation length. Charge transport measurements showed a mobility increase with decreasing chain length. We correlated the molecular packing and morphology to charge transport and determined that carrier mobilities are most sensitive to crystallinity and crystal grain misorientation. This indicates that molecular weight is not a decisive factor for improved carrier mobility in the low molecular weight region, but rather the degree in crystallinity and in-plane crystal orientation. These results represent a fundamental advancement in understanding the relationship between conjugation length and carrier mobilities in oligothiophene semiconductors.
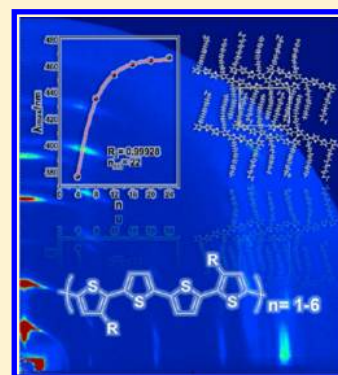
INTRODUCTION

Polythiophenes have become the benchmark polymer semiconductor material in high-performance devices, such as organic field-effect transistors and organic photovoltaics.[1−4] There has been tremendous effort over the years to study these materials in the solid state and understand how molecular structure is linked to device performance and to charge transport mechanisms.[5−11] However, polythiophenes exhibit complicated morphologies owing to the intrinsic complexities of polymeric solids and their inability to fully crystallize like small molecules.[12] As such, crystallization in polymers is "frustrated" by the entropic barriers associated with chain entanglements and chain folding. It is further aggravated by the stiff backbones and long side chains that are characteristic for conjugated polymers, such as polythiophenes.[12] Structure−property investigations have been limited because of persistent problems which often include lack of crystallinity, intrinsic disorder, broad polydispersity, and defects. In contrast, low molecular weight polymers, or oligomers, are easier to

crystallize and serve as information-rich sources for understanding solid-state packing of polymer analogs.[13−22]

Monodisperse oligomers with well-defined and uniform chemical structures have recently been explored in attempts to extrapolate the properties of the corresponding high molecular weight polymer analogues.[13−22] Oligothiophenes with 96-mers and oligofluorenes with 64-mers have been synthesized, and their properties were correlated to their polymers.[17,18] There are also ongoing efforts in functionalizing oligomers with heteroatoms for high-performance organic semiconductor devices. Organoborane and furan moieties have been incorporated into the backbone of oligomers for applications in optoelectronics and "green" organic devices.[23,24] Bäuerle and co-workers synthesized a 12-unit oligomer of 3,3′″-didodecyl-2,2′:5′,2″:5″,2′″-quaterthiophene (DDQT) and determined the crystal structure.[19,20] The 12-unit oligomers were found to have a markedly different structure and intermolecular

Scheme 1. Synthetic Steps to the Oligothiophenes (DDQT 1-6).[a]
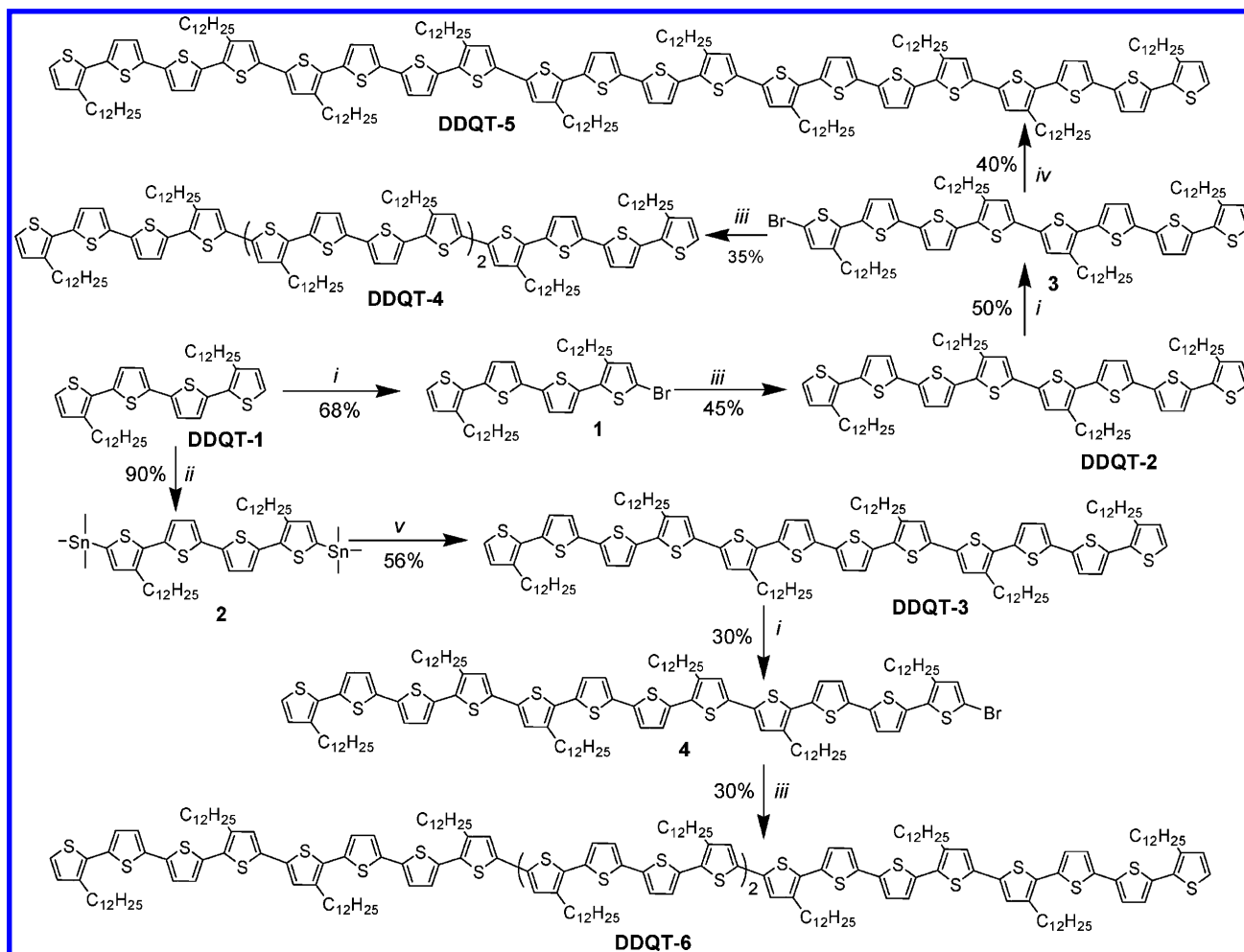
[a]Reagents and Conditions: (i) NBS, AcOH/chloroform (1:1), 0 °C to room temperature; (ii) BuLi, trimethyltin chloride, THF, −78 °C to room temperature; (iii) bis(tri-n-butyltin), Pd(PPh$_3$)$_4$, toluene, 115 °C; (iv) **2**, Pd(PPh$_3$)$_4$, toluene, 115 °C; (v) **1**, Pd(PPh$_3$)$_4$, toluene, 115 °C;

interactions than the previously characterized 4-unit monomer of DDQT. In a separate study, thin-film transistors were fabricated from low molecular weight fractions of poly(3,3′″-dialkyl-quaterthiophene) (PQT-12) isolated by Soxhlet extraction.[25] It was found that mobility increased with chain length, except at the lowest molecular weight studied, which exhibited mobility nearing that of the high molecular weight PQT-12. The authors attributed the mobility to the narrow polydispersity, which is crucial in forming highly ordered, micrometer-sized crystalline domains.

This work is motivated by the need to understand how varying the chain length of thiophene oligomers directly affects the electronic structure, crystal structure(s), thin-film morphology, and charge transport properties. We report the synthesis of pure DDQT oligomers from 4 to 24 thiophene rings and determine the electronic, molecular, morphological, and charge transport properties. An important result from this study is the ability to extrapolate the convergence for increasing numbers of thiophene units to the limiting value of the corresponding polymer (PQT-12) and a morphology evolution from small molecule-like packing to polymer-like packing in thin films occurring near the point where the effective conjugation length is reached. Any further extension of the chain is presumed to no longer effect a certain property (i.e., HOMO−LUMO or band

gap) of the corresponding polymer, but film morphology and device performance are still effected. These results show a fundamental advancement in understanding the relationship between conjugation length, film morphology, and carrier mobilities in oligothiophene semiconductors.

■ RESULTS AND DISCUSSION

Synthesis and Molecular Characterization. As shown in Scheme 1, our synthetic strategy relies on the divergent−convergent approach to conjugated oligomers, which affords monodispersed molecular systems with facile isolation and purification. Oligothiophenes were synthesized via palladium-catalyzed Stille reactions between successive brominated and stannyl intermediates. A detailed description of the synthesis is available in the Supporting Information (SI). The oligomers are soluble in common solvents, such as chloroform, THF, and toluene, and were purified by silica column and recrystallized in different solvents, thus avoiding the use of HPLC. The molecular structures of all oligomers were unambiguously characterized by MALDI-TOF and ^{1}HNMR. Although GPC showed larger molecular weights than the theoretical value due to the rod-like nature of the oligomers compared to the coiled-like polystyrene standard, the very low polydispersity indices (PDI = 1.01−1.02) confirmed the oligomer purity (Figure 1).
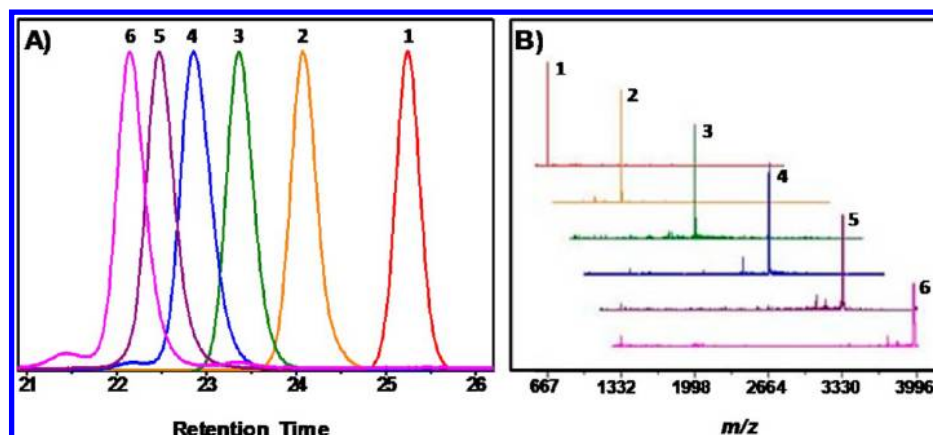
Figure 1. (A) GPC traces of oligothiophenes (DDQT 1−6) (THF vs PS standard) and (B) MALDI-TOF spectra of oligothiophenes (DDQT 1−6) (terthiophene as the matrix).
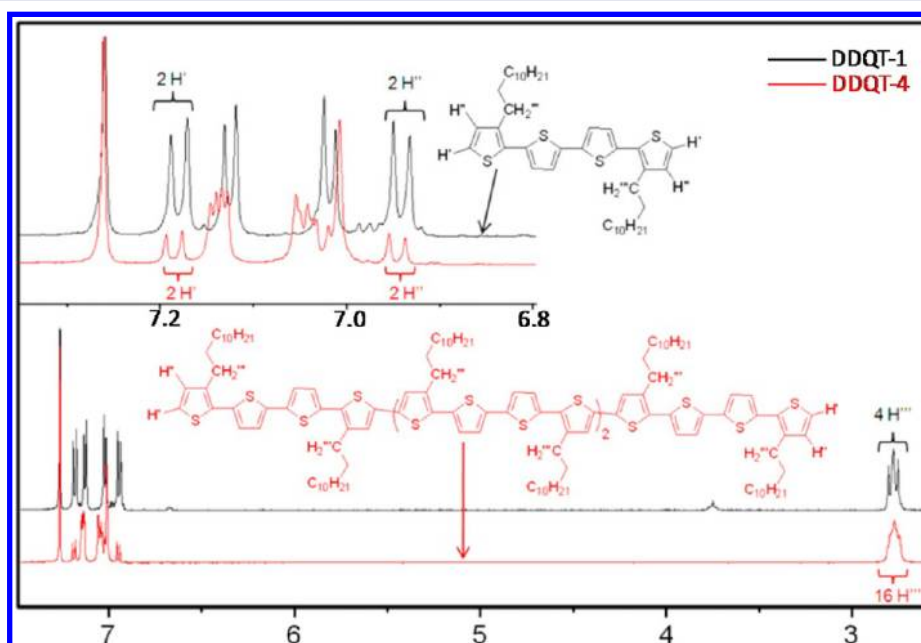

Figure 2. Representative ^{1}HNMR spectrum showing the signal for DDQT-1 and DDQT-4 (CDCl$_3$, 25 °C).
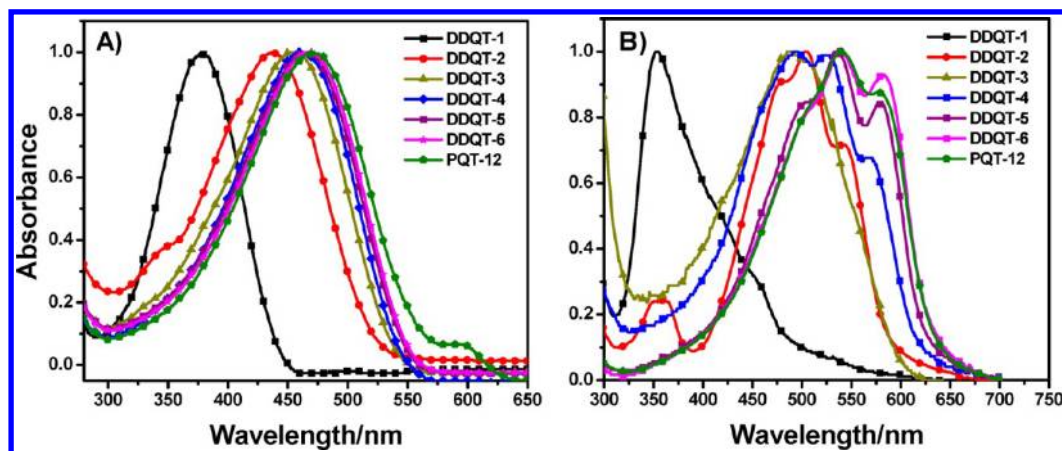

Figure 3. UV−vis spectra of oligothiophenes (DDQT-1−6) in (A) chloroform and (B) thin films on glass.

It should be noted that the structure determination is also confirmed via ^{1}HNMR and the overall integration ratio between the aliphatic protons and the aromatic protons (Figure

2). The ratio between the protons at σ 6.90, assigned to the two β-thiophene protons, and the protons corresponding to the methylene groups is dependent on the length of the oligomers,

which increases by an integration factor of 4 for every consecutive building block (i.e., $n = 1-6$).

Electronic Structure, Optical, and Redox Properties. The absorption spectra of the oligothiophenes in chloroform are shown in Figure 3A. As expected, the spectra are featureless, and there is a large red-shift of the maximum absorption from DDQT-1 to DDQT-4 with increasing molecular weight. However, there is only a minor red-shift from DDQT-5 to DDQT-6 and the polymer (PQT-12). In the short oligothiophene series, there is a linear relationship between the energy of the long-wavelength transition [E_{abs} (eV)] and the inverse of the oligomer length [$1/n$], but there is a deviation from linearity with increasing oligomer length due to the occurrence of saturation, which is defined as the effective conjugation length (ECL) (Figure 4A).[26−29] It has been shown
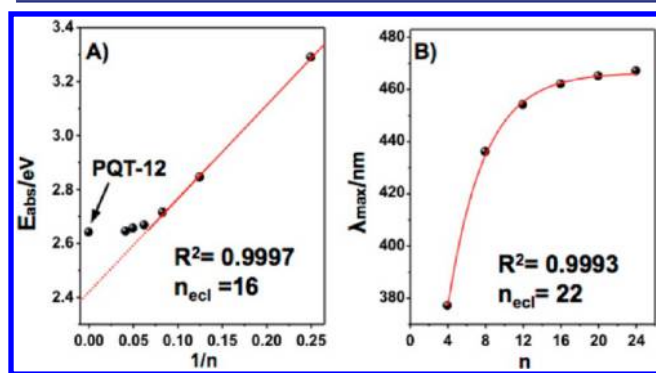

Figure 4. (A) Correlation between absorption energies (E_{abs}) and inverse numbers ($1/n$) of oligothiophenes (DDQT-1−6) and (B) absorption maximum vs oligothiophene units.

that there is an empirical relationship between the absorption energy and the inverse number of thiophene units for a chain length of up to eight rings. The linear relationship of the transition energy is, $E(eV) = 3.48/n + 2.42$, where the slope is close to that for nonsubstituted oligothiophenes (3.76).[29] It is possible to estimate the ECL from the oligothiophene series by extrapolating the linear region of the plot of absorption energies to the value of the polymer with the infinite length. With the limiting absorption maximum of 470 nm measured for the high molecular weight PQT-12 ($M_n = 28K$), the linear extrapolation of the plot in Figure 4A would suggest an ECL of approximately 16 thiophene rings or $n = 4$ (i.e., DDQT-4). Although a linear correlation (regression coefficient = 0.9997) exists when one extrapolates to the infinite long chain, a value of 2.41 eV is obtained which corresponds to $\lambda_{max} = 515$ nm. This absorption energy is much larger than the value of 470 nm

measured for the high molecular weight PQT-12, which suggests that a linear fit is a close approximation but not appropriate in the high molecular weight range and/or for the longer oligomers. This result is consistent with the study of Meier et al., who suggested that an exponential fitting of the wavelength (λ, nm) versus number of repeat units (n) is more appropriate for oligomers, as it takes into account the convergent behavior of the maximum absorption when reaching relatively large numbers of repeating units.[28] The effective conjugation length can be expressed as:

$$\lambda_{max}(n) = \lambda_\infty - (\lambda_\infty - \lambda_1)e^{-b(n-1)}$$

$$n_{ecl} = \frac{\ln(\lambda_\infty - \lambda_1)}{b} + 1$$

In applying this model to the absorbance data, we find that the limiting wavelength of high molecular weight polymer, λ_∞, is 470 nm, the absorbance of a single thiophene monomer, λ_1, is 278 nm, and the convergence factor b is 0.246. This fitting leads to an ECL of ∼22, which roughly corresponds to the oligomer length of DDQT-5 (20 thiophene units) and is larger than the value calculated via the linear extrapolation model.

Figure 3B shows the absorption spectra of the thin films of oligomers on glass. In general, there are consistent red shifts of the absorption spectra in the solid state compared to in solution due to more planar conformations and stronger interchain interactions.[30] However, DDQT-1 displays a large blue-shift in the solid state, suggesting H-aggregation. The thin film of DDQT-2 exhibits a very narrow absorption spectrum, and there is a small red shift relative to the film of DDQT-3, which exhibits a rather broad absorption in the solid state due to a twisted backbone and multiple intermolecular interactions. This red shifting is in agreement with the observation by Neher and co-workers.[25] Interestingly, from DDQT-4 onward, these longer oligomers exhibit a small red-shift and well-structured absorption with increasing molecular weight. This pronounced vibronic transition could be interpreted as aggregation in the solid state in which highly ordered structures form due to interchain interactions.[31] We observed that from DDQT-5 onward, the absorption energy appears to behave independently with increasing molecular weight but exhibits slightly different intensity corresponding to the 0−0 transition (580 nm) of π−π* absorption at about 2.13 eV. The peak ratio of the 0−0 and 0−1 transitions can be correlated with the conjugation length and the crystal quality.[31−33] The higher ratio measured here suggests a longer conjugation length and a higher crystal quality.

Table 1. MS, GPC, Optical Properties, and Electrochemical Data of Oligothiophenes (DDQT-1−6)

compd	MS_{calc} (m/z)	MS^a (m/z)	GPC^b (Mn)	PDI	ε (L mol^{-1} cm^{-1})	λ_{max} [nm]^c solution	λ_{max} [nm]^d thin film	$E_{HOMO}{}^e$ [eV]	$E_g{}^f$ [eV]	$E_g{}^g$ [eV]
DDQT-1	667.15	666.60	649	1.01	25844	378	355	5.27	2.82	2.59
DDQT-2	1332.67	1334.55	2284	1.01	57775	436	478, 506, 542	5.13	2.31	2.14
DDQT-3	1997.41	1997.58	4694	1.01	92594	457	492	4.97	2.30	2.11
DDQT-4	2662.15	2664.49	6456	1.02	136968	465	491, 523, 568	4.92	2.28	2.03
DDQT-5	3327.68	3329.13	7404	1.01	162722	468	538, 580	4.90	2.26	1.96
DDQT-6	3992.18	3994.23	10753	1.02	181922	470	540, 580	4.87	2.25	1.96

^{a}MS molecular weights were measured by a MALDI-TOF mass spectroscopic instrument using terthiophene as the matrix. ^{b}GPC molecular weights were determined with the polystyrene standard in THF. ^{c}Absorptions were measured in chloroform. ^{d}Absorptions were measured in thin films on glass. $^e E_{HOMO}$ determined by CV in THF solution. ^{f}Estimated from solution absorption onset. ^{g}Estimated from thin-film absorption onset.
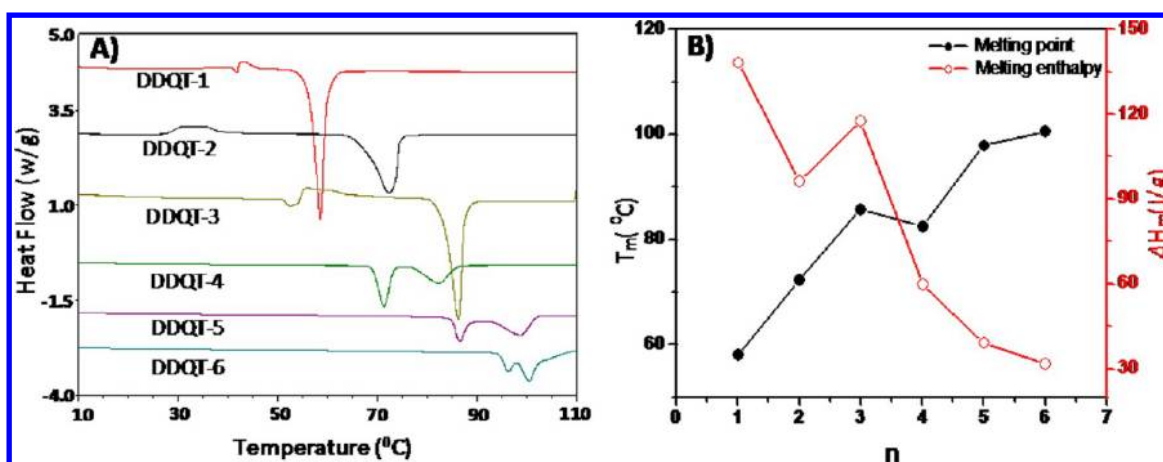
Figure 5. (A) DSC heating process with a rate of 10 °C/min and (B) melting points and melting enthalpies (ΔH_m), from the oligothiophene powder samples measured by DSC as a function of oligomer number.

Cyclic voltammetry (CV) studies were performed in THF to estimate the energy levels of the oligothiophenes, with 0.1 M TBAPF$_6$ as the supporting electrolyte at a scan rate of 100 mV/s. The highest occupied molecular orbital (HOMO) energies, i.e., the oxidation onset, were measured between 5.27 and 4.87 eV, and the HOMO−LUMO gaps obtained from the absorption onsets vary from 2.82 to 2.25 eV. From DDQT-1 to DDQT-6, the first oxidation potentials gradually decrease to saturation with increasing chain length as summarized in Table 1, and the convergence of the HOMO level for oligomers longer than DDQT-3 was experimentally observed.

Melting Behavior and Thermal Properties. The thermotropic properties of the oligomers were characterized by differential scanning calorimetry (DSC) (Figure 5A) and summarized in Table 2. From DDQT-4, the DSC thermogram

Table 2. Thermal Properties of the Oligothiophenes

compd	T_m (°C)		T_c (°C)		area of melting (J/g)	
DDQT-1	58.59		17.71		138.30	
DDQT-2	72.34		15.85		96.46	
DDQT-3	86.39		29.06		117.70	
DDQT-4	71.29	84.53	53.49		32.66	27.19
DDQT-5	86.39	98.98	68.40		14.61	24.67
DDQT-6	95.95	100.67	77.68		7.15	24.72

showed liquid crystalline characteristics with two endotherms, corresponding to the crystalline-to-liquid crystalline and liquid crystalline-to-isotropic phase transitions, respectively.[34,35] We observed that with increasing chain length, the crystallization temperature (T_c) increased, and the melting enthalpies decreased, however, DDQT-2 exhibited a lower crystallization temperature than that of DDQT-1, partially due to the frustrated alkyl chain folding.[31] In Figure 5B, ΔH_m is plotted with *n*. It is apparent that the slope of the melting enthalpy between DDQT-3 and DDQT-4 is steep. From DDQT-4, the melting enthalpy decays much slower and tends to saturate with molecular weight increase. In fact, the melting enthalpy decreases by about 58 J/g from DDQT-3 to DDQT-4. The interpretation of this data is that DDQT-4 is more difficult to crystallize and has a lower crystallinity compared to DDQT-3. By examining the enthalpy−molecular weight decay profile and data summarized in Table 2, one can conclude that crystallinity decreases with molecular weight increase, with DDQT-2 as a

notable exception. This result further suggests that the crystallization behaviors of these linear oligothiophenes are strongly influenced by the molecular size, where the shorter molecules are more easily crystallized. Although it is difficult to interpret variations in melting points (T_m) among the oligothiophenes, it is natural to conclude that the longer oligomers show much richer crystal morphologies due to the conformational complexity of the elongated chains and increased number of side chains, as directly evidenced by the new emerging liquid crystal-forming phase starting from DDQT-4. Importantly, the sharp change in melting enthalpy from DDQT-3 to DDQT-4 indicates that it is at around this molecular length that the molecular properties shift from small molecule to macromolecules.

Structure Analysis, Crystal Packing, and Film Morphology. Single crystal structure determination affords a systematic investigation of how the chain length controls the solid-state structures of oligothiophenes. From DDQT-1 to DDQT-3, the values of C−C bonds length, C=C double bonds, and chain length alternation are quite comparable with those of other alkylated oligothiophenes.[36] However, there is a distinct difference in backbone planarity and thiophene configuration. In DDQT-1, the thiophene rings display an *anti* conformation to each other. The torsion angle of the two thiophenes located at the external and internal positions are 12.2° and 0°, respectively (Figure 6A).[19] For DDQT-2, the eight α-linked rings in the backbone exhibit *anti* conformations except for the two outermost rings, which display *syn* conformations, and the torsion angle between the outer thienyl and inner thienylene rings is close to 3.5°. This *syn* conformation is also observed in DDQT-3, with a larger torsion angle.[20] In particular, the torsion angles in DDQT-3 are as large as 60°, while the torsion angle in DDQT-2 are on the order of 7−8° (Figure 6B,C). This deviation from planarity is due to the steric interactions between the alkyl chains and the adjacent thiophene rings.

Compared to the unsubstituted oligothiophene (i.e., α-4t, α-6t, and α-8t), which all crystallize in the same monoclinic space group and display herringbone arrangement due to strong edge-to-face interactions, the crystal packing of substituted oligothiophenes can arise from not only the backbone organization but also side chain conformation.[37−41] DDQT-1 and DDQT-3 form lamella-type packing motifs by self-assembly through the π−π interactions together with the
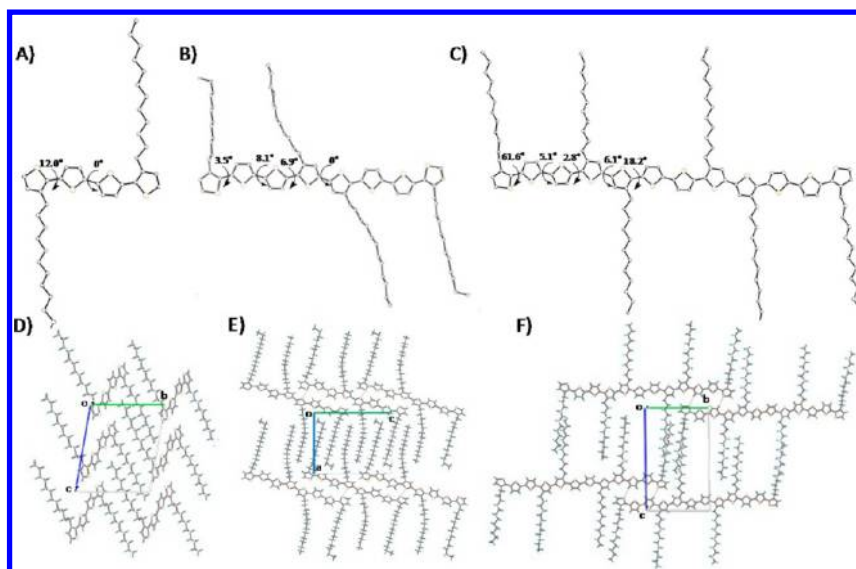
Figure 6. Crystal structure and oligothiophene conformation of (A) DDQT-1, (B) DDQT-2, and (C) DDQT-3. Crystal packing, alkyl chain interdigitation of (D) DDQT-1 along *a*-axis, (E) DDQT-2 along *b*-axis, and (F) DDQT-3 along *b*-axis. (Crystal structures of DDQT-1, DDQT-3 are reported in refs 19 and 20).
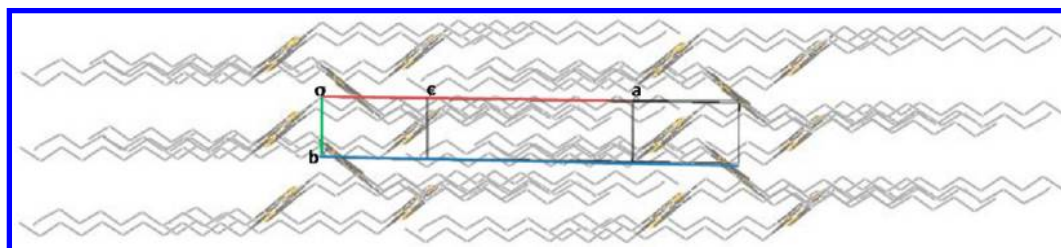

Figure 7. Herringbone packing and alkyl chain interdigitation of DDQT-2. Hydrogens were omitted for clarity.
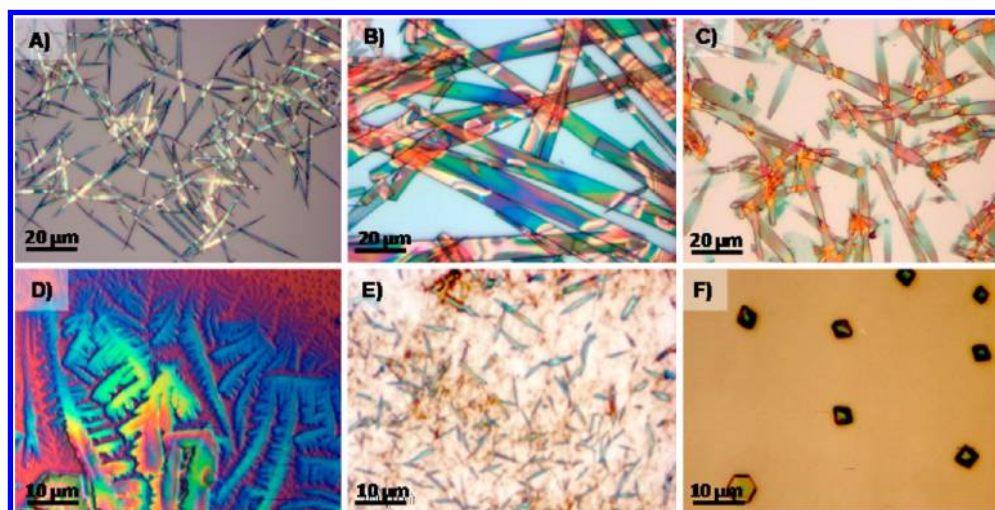

Figure 8. Optical images of oligothiophene single crystals. (A) DDQT-1, (B) DDQT-2, (C) DDQT-3, (D) DDQT-4, (E) DDQT-5, and (F) DDQT-6. Crystals in (A−C) were grown from hexane/ethanol mixture and (D−F) were grown onto Si substrates over one week via slow evaporation of chloroform.

intermolecular hydrophobic interaction between alkyl chains.[19,20] Along the *a*-axis, DDQT-1 forms a 2-D lamella-type packing with one thiophene ring overlapped, and there are no heteroatomic interactions (Figure 6D).

DDQT-3 packs in a lamellar structure, with four terminal thiophene rings of the oligomers overlapping and linked by multiple intermolecular contacts between the C−H, S−H, and

H−H interactions (Figure 6F). Interestingly, DDQT-2 crystallizes in a "lamellar herringbone" packing motif with half of the backbones overlapping and locked together by C−H and S−S interactions and with a relatively large angle of 85° (Figures 6E and 7). The structure has herringbone-like stacks that are arranged in layers separated by the alkyl chains (Figure 7). For comparison, α-8T packs in herringbone geometry with
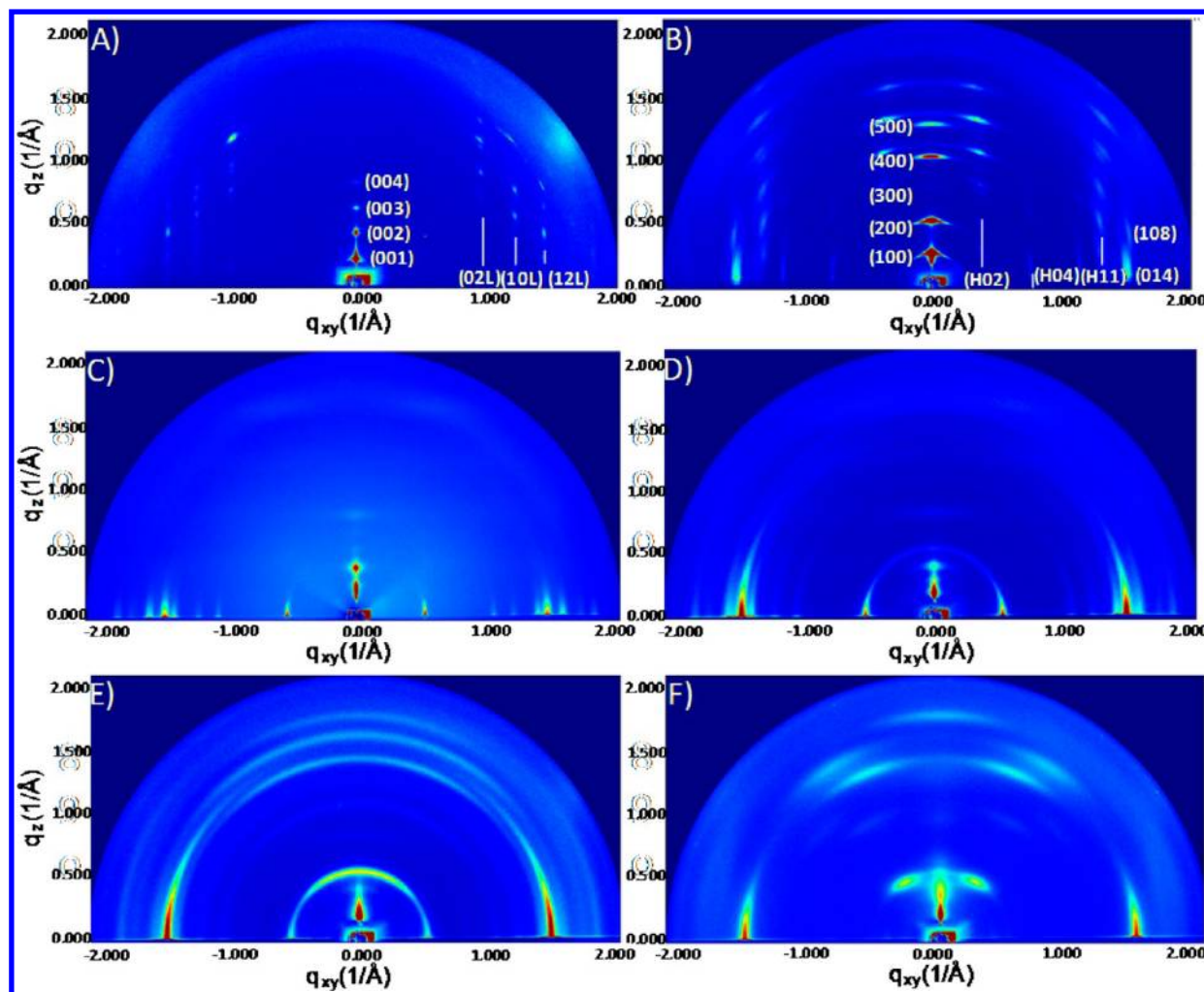
Figure 9. GIXD images of oligothiophenes on Si substrate by spin-cast from chlorobenzene solution: (A) DDQT-1, (B) DDQT-2, (C) DDQT-3, (D) DDQT-4, (E) DDQT-5, and (F) DDQT-6.

two different polymorphs and has a rigorously planar all-*trans* conformation, with a dihedral torsion angle <1°. It should be noted that there are large roll angles 60.7° and 58.4°, respectively, in α-8T, which suggest that adjacent molecules in a stack slip out from each other and that there is no π−π stacking.[42] In DDQT-2, the roll angle is about 32°, resulting in substantial spatial overlap between the adjacent molecules within a π-stack. Compared to DDQT-1 and DDQT-3 with almost fully extended side chain conformations, DDQT-2 has a bent side chain conformation with only the α-carbon perpendicular to the backbone and the other carbons extended out of the backbone with a torsion angle of ~117° (Figure S5). The last carbons of two side chains are bent parallel to the molecular backbone due to the C−H intermolecular repulsion between the alkyl chain and thiophene rings. Finally, it should be noted that there is partial overlap between the backbones in the crystals of DDQT-2 and DDQT-3. This overlap results in a significant electronic coupling between adjacent molecules, which is beneficial for charge transport.

Figure 8 shows optical images of oligothiophene crystals on Si substrates. DDQT-1−3 easily form large single crystals from ethanol:hexane (4:1) solutions. The crystals have lengths ranging from 5 μm to well over 1000 μm and average widths from 1 to 20 μm. We found it more difficult to form large crystals from the longer oligothiophenes. Nevertheless, crystal

formation was possible by slow evaporation/crystallization over several days.

It is well-known that the molecular packing in thin films can significantly differ from the bulk crystal structures. Grazing incidence X-ray diffraction (GIXD) is the only scattering geometry that can provide details about the crystalline packing in thin films of weakly scattering organic semiconductor materials.[43−47] With GIXD, the molecular packing can be probed in both the out-of-plane (q_z) and in-plane (q_{xy}) directions. GIXD experiments were performed on thin-film samples of oligothiophenes to further study the influence of the increasing length in the oligomers on the resultant thin-film morphology. Figure 9 shows the GIXD pattern of oligothiophene films spin coated on Si substrates. The diffractograms of ~40 nm thick DDQT-1 and DDQT-2 thin films in Figure 9A show that the diffraction peaks are aligned vertically (forming so-called Bragg rods) indicating that the crystalline grains are aligned with the substrate plane, with a random azimuthal orientation in the substrate plane ("2D powder"). It is difficult to unequivocally index this diffraction pattern, but the visible Bragg peaks are compatible with an in-plane unit cell ($a = 5.04$ Å, $b = 12.85$ Å, $\gamma = 98.3°$) that is similar to the $a−b$ plane of the DDQT-1 bulk unit cell (Figure 7D, $a = 5.59$ Å, $b = 12.27$ Å, $\gamma = 100.7°$). The d_{001} spacing of this DDQT-1 thin-film phase (31 Å) is also roughly twice as long as the corresponding crystal

spacing (14 Å). This indicates that the DDQT-1 thin film is less ordered than the crystal with likely more molecules in the unit cell. For DDQT-2, the absence of the first two in-plane diffraction orders is consistent with the herringbone-like arrangement of the molecules in the bulk. The d_{100} spacing of the DDQT-2 film (24.15 Å) is almost identical to the corresponding lattice parameters for bulk crystal (24.7 Å). The peaks at q_z = 0.26, 0.52, 1.02, 1.28 correspond to d spacings of 24.15, 12.07, 6.15, and 4.90 Å, which are in good agreement with the values for the (100), (200), (400), and (500) reflections from powder XRD. These peaks indicate the molecule is nearly standing on the substrate with the bc plane parallel to the substrate surface. Indeed, the in-plane diffraction peaks can be indexed with a unit cell (b = 4.67 Å, c = 32.70 Å, α = 87.4°) that is very similar to the bulk $b-c$ plane cell. The scattering pattern of DDQT-3 is drastically different from that of DDQT-2. This is possibly due to the difference in symmetry; DDQT-2 has a lower molecular symmetry with respect to its side chains than DDQT-3, which is likely responsible for a significantly different molecular packing motif. In DDQT-3, there is only weak lamellar stacking order, indicated by the occurrence of only a single weak peak of the 00L rod, located at q_z= 0.40 Å^{-1}. More importantly, the DDQT-3 diffraction image marks a transition point in the series; most of the small-molecule characteristics have disappeared. Most importantly, the Bragg peaks that appear in the shorter oligomers of the series are characteristically arranged as vertical rods. Compared to DDQT-2, the peaks from DDQT-3 are quite close to the horizon indicating that most of the crystalline order is confined to planes parallel to the substrate with very little or no out-of-plane order left. Furthermore, a set of four characteristic peaks (q = 0.55, 1.42, 1.50, 1.62 Å^{-1}) first appears in the DDQT-3 diffraction images—exclusively as in-plane peaks—and also dominates the diffraction images of DDQT-4,5,6. In the corresponding polymer PQT-12, the peak at 1.62 Å^{-1}, with a corresponding d-spacing of 3.87 Å, is typically referred to as the $\pi-\pi$ stacking peak.[48] In DDQT-4, there is significant arching in these peaks and generally an onset of powder ring formation, indicating that the individual grains are no longer aligned with the substrate surface plane but instead more randomly oriented. The arching in these peaks increases going from DDQT-4 to DDQT-5. However, in DDQT-6 these peaks are more discrete again, suggesting that the longer DDQT-6 molecules have a higher degree of orientation relative to the substrate surface than DDQT-5. Unlike in DDQT-3 and DDQT-4 though, these peaks are not predominantly located in the substrate plane. Most notable is the fact that the $\pi-\pi$ stacking peak lies no longer in the substrate plane which is detrimental to the charge transport properties of DDQT-6 films. While films of DDQT-3 and DDQT-6 are quite similar in the observed lattice spacings, the DDQT-6 texture of crystalline grains is very different from that found in DDQT-3 and DDQT-4, whereas almost no texture is present in DDQT-5 films at all. In summary, the 2D diffraction patterns of these compounds indicate that the conjugation length has a tremendous effect on the overall film morphology of the oligomers, which are different from that of PQT-12 on the substrate.[48]

Charge Transport Properties. Electrical measurements were performed in ambient conditions using a standard probe station. Thin film OFETs are fabricated in a "top contact" geometry by spin-coating 10 mg/mL solution of oligothiophenes in chlorobenzene at 2000 rpm for 30 s. The hole mobilities calculated in the saturated regime, threshold voltages,

and current on/off ratios are summarized in Table 3. DDQT-2 transistors exhibited the highest device performance, with

Table 3. Mobility, On/Off Ratio, and Threshold Voltage of the Oligpthiophene Devices

compd	mobility (cm^{2}V^{-1}S^{-1})	on/off	V_{th} (V)
DDQT-1	NA	NA	NA
DDQT-2	$(1.0-4.3) \times 10^{-3}$	$(0.5-5.5) \times 10^3$	$-0.9-0.6$
DDQT-3	$(1.7-2.6) \times 10^{-3}$	$(0.9-1.3) \times 10^3$	$-0.9-0.6$
DDQT-4	$(1.8-2.7) \times 10^{-4}$	$(0.4-1.0) \times 10^3$	$0.7-1.5$
DDQT-5	$(1.3-4.6) \times 10^{-4}$	$(0.3-2.8) \times 10^3$	$3.4-7.4$
DDQT-6	$(0.86-1.1) \times 10^{-4}$	$(0.1-1.3) \times 10^3$	$-7.1\sim-8.2$
DDQT-3[a]	$0.01-0.04$	$(1.0-4.0) \times 10^3$	$-1.3-6.7$

[a]Single crystal transistor.

mobilities of ~4.3 × 10^{-3} cm^2 V^{-1} s^{-1} and current on/off ratios of ~10^3. The mobilities are comparable with that reported by Neher et al.[25] The strong 2D intermolecular coupling in the substrate plane in DDQT-2 results in a film morphology that contains large crystallites, as is necessary for efficient charge transport. The slipped herringbone packing in the substrate plane results in a large orbital overlap between neighboring molecules in the charge transport direction. Thin film transistors fabricated from DDQT-3 show mobilities up to 2.6 × 10^{-3} cm^2 V^{-1} s^{-1}, which is attributed to highly oriented crystals with lamellar packing in the film. In contrast, DDQT-4−6 show lower carrier mobilities on the order of ~10^{-4} cm^2 V^{-1} s^{-1}. These values are 3 orders of magnitude lower than that of PQT-12. These results are explained by poorly oriented crystals and the random orientation of the molecules in the thin films (in the case of DDQT-4 and especially DDQT-5), which is unfavorable for charge transport. In DDQT-6, the $\pi-\pi$ stacking direction does not lie in the substrate plane which limits carrier transport through the molecular solid.

Field-effect transistors based on DDQT-3 crystals were also fabricated and characterized (Figure 10). The single crystals were prepared from a hexane solution of DDQT-3 by the slow addition of ethanol (SI). The crystal structure and molecular arrangement are characterized by transmission electron microscopy (TEM). Figure 11 shows a single crystal with the corresponding electron diffraction and simulated reciprocal lattice diffraction. We observed a remarkable similarity in diffraction between the observed and "calculated" patterns. The a and b lattice constants were determined to be 9.191 and 13.558 Å, respectively, with the a and b vectors enclosing an angle γ of 66.1°. These values are in agreement with those found by Azumi et al. of 9.617 Å, 13.895 Å, and 72.9°, respectively.[20] Additionally, the geometry of the reciprocal unit cell indicates that the long axis of the crystal corresponds to the [100], i.e., $\pi-\pi$ stacking, direction (real space packing). This is in agreement with a common finding in organic crystalline 1D nanostructures, namely that the direction of greatest orbital overlap is also the direction of fastest growth.[49,50] We obtained mobilities in the range of ~0.04 cm^2 V^{-1} s^{-1}, with an on/off current ratio of ~10^4. These results are comparable to those reported for thin-film transistors based on PQT-12 without postannealing and 1 order of magnitude higher than that of the DDQT-3 thin-film transistors due to the reduced number of crystal defects and grain boundaries.

The electrical performance in oligomer OFETs is determined by several factors, including molecular packing in the crystalline grains, grain sizes, and degree of crystallinity inside the grains
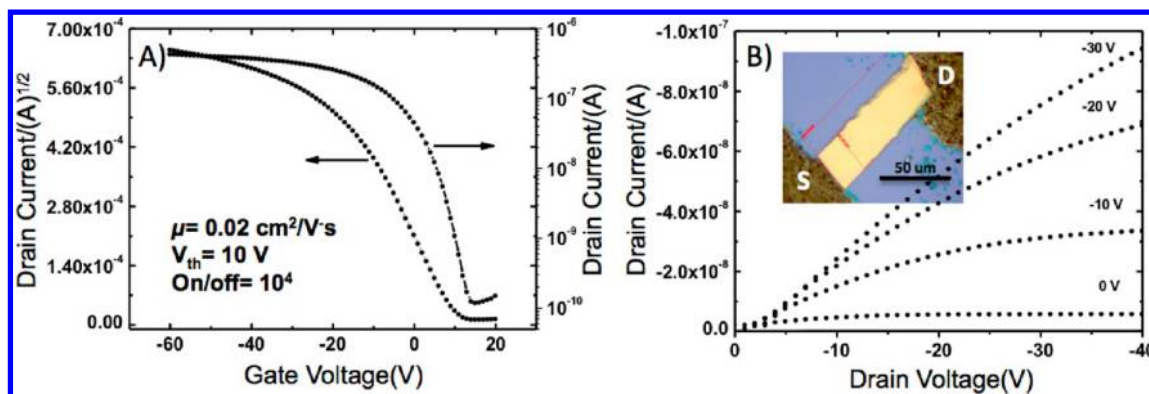
Figure 10. (A) The transfer/square root of current characteristics and (B) output characteristics of a DDQT-3 single crystal transistor. Inset: single crystal transistor of DDQT-3 on Si/SiO$_2$ (300 nm) with carbon paste as top-contact source-drain electrodes.
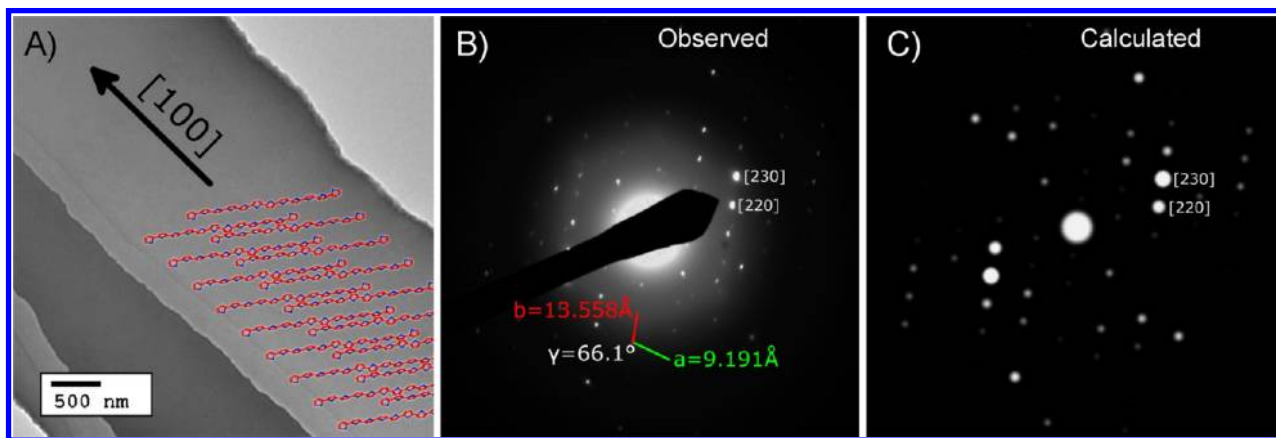

Figure 11. (A) TEM of a DDQT-3 single crystal with elucidated molecular packing overlay, (B) the corresponding diffraction image with measured *a*- and *b*-unit cell dimensions, and (C) the "calculated" electron diffraction pattern generated from the bulk structure refinement data using CrystalMaker software, Ltd.
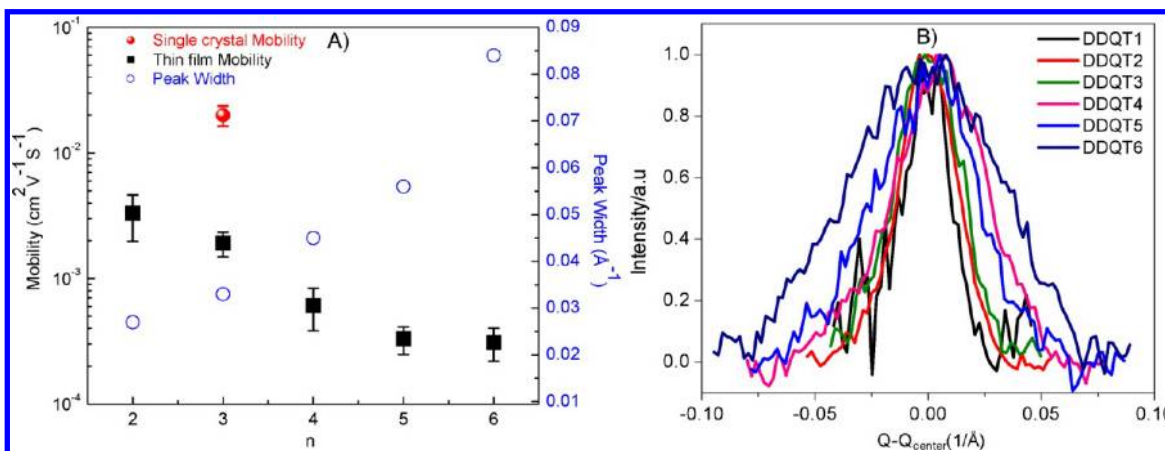

Figure 12. (A) Thin-film carrier mobilities of oligothiophenes (black squares) and in-plane peak widths (open circles) as a function of oligomer length. A single crystal transistor of DDQT-3 is shown in red circles. (B) Overlay of the evolution of the peak width at $|q| = 1.0$ Å^{-1} that can be found in the oligothiophene diffraction pattern series. The data shows a significant decrease in crystalline order with increasing oligomer length.

or, conversely, the density of packing defects.[51−56] Since the conducting channel in OFETs forms in a few layers directly above the interface to the dielectric, the degree of in-plane crystalline order is particularly important. The GIXD images of the DDQT series show significant changes in the lattice and, consequently, the molecular packing with a difficult to quantify impact on the measured OFET performance of the series (decreasing mobility with increasing oligomer length).

However, one trend that can be identified in the GIXD images and which is related to OFET performance is the evolution of the in-plane scattering peak width as function of the oligomer length (Figure 12 A).[54,55] In GIXD experiments on polycrystalline thin films, the observed peak width is the rather complicated result and convolution of multiple peak broadening mechanisms: size broadening, paracrystalline disorder broadening, and broadening due to the beam footprint on the

I

dx.doi.org/10.1021/ja3104796 | *J. Am. Chem. Soc.* XXXX, XXX, XXX−XXX

sample.[54] The peak widths plotted in Figure 12 B were measured for in-plane peaks at the same position near 1.0 Å^{-1}. Evolution of the peak width close to $|q| = 1.0$ Å^{-1} can be found in all diffraction patterns. The broadening of a peak that is located at a fixed q in a set of samples of very similar size, and thus sample beam footprint, is directly related to the differences in crystallographic coherence length. The peak becomes broader when the length scale over which the material is crystalline becomes smaller. The data therefore show a significant decrease in crystalline order with increasing oligomer length. Though, as stated above, we cannot account for the differences in the molecular packing in the DDQT series, the observed trend of increasing peak widths with oligomer length is consistent with the corresponding decrease in the measured OFET hole mobility. The additional information on morphology of the thin films was investigated by atomic force microscopy (AFM) (SI). The DDQT-2 and DDQT-3 films have large crystallites with fewer grain boundaries. However, the film topography of DDQT-4 and DDQT-6 was rather featureless, and we suspect that films are mixtures of small crystal grains and amorphous domains. DDQT-5 films exhibit well-defined nanostructures, however there appears to be a high degree of misorientation between the nanostructures.

CONCLUSION

We have synthesized a series of monodisperse oligothiophenes based on didodecylquaterthiophene (DDQT). The synthesis described here, involving end-functionalization of oligomers, is general and should permit construction of even longer oligothiophenes as well as the synthesis of other well-defined conjugated polymers. In this contribution, we emphasize the key role of the conjugation length on the electronic properties, the degree of crystallinity, and the thin-film morphology. A comparative investigation of the optical absorption, thermal properties, electrochemical potentials, and thin-film morphologies of the oligothiophenes clearly indicates that the conjugation length plays a major role in controlling the fundamental electronic properties. The empirical approach for extrapolating the convergence predicted 16 thiophene units. However, this method is found to be inaccurate, as it does not consider the absorption of the infinite polymer. In contrast, the exponential fit model that considers the limiting value of the polymer and the difference between it and the thiophene repeat unit yields an ECL of 22 thiophene units. The oligomers DDQT-1 and DDQT-2 crystallize in a "2D powder," as expected for small molecule polycrystalline thin films. GIXD measurements indicate an evolution from small molecule-style packing to polymer-style packing occurs near the effective conjugation length. Our data suggest that the molecular weight is not a decisive factor for improved carrier mobility in the low molecular weight region, and increasing in-plane lattice disorder with increasing chain length contributes to the decreased carrier mobilities.

In all aspects, this work presents an important advancement to understanding the detailed structural information, crystallinity/morphology, and charge transport of oligothiophenes as a function of chain length. The oligothiophenes reported here will serve as important model systems for understanding electrical, optical, optoelectronic, and theoretical properties of the corresponding polymer.

ASSOCIATED CONTENT

S **Supporting Information**

Detailed synthesis and characterization of DDQT 1−6; ^{1}HNMR, and ^{13}CNMR of the oligomers, crystal structure data for DDQT-2, DSC, and electrochemistry. This material is free of charge via the Internet at http://pubs.acs.org.

AUTHOR INFORMATION

Corresponding Author
abriseno@mail.pse.umass.edu
Notes
The authors declare no competing financial interest.

ACKNOWLEDGMENTS

REFERENCES

(1) Beaujuge, P. M.; Fréchet, J. M. J. *J. Am. Chem. Soc.* **2011**, *133*, 20009−20029.
(2) Thompson, B. C.; Fréchet, J. M. J. *Angew. Chem. Int. Ed.* **2007**, *47*, 58−77.
(3) McCullough, R. D. *Adv. Mater.* **1998**, *10*, 93−116.
(4) *Electronic Materials: The Oligomer Approach*; Müllen, K., Wenger, G., Eds.; WILEY-VCH: Weinheim, Germany, 1997.
(5) Kline, R. J.; McGehee, M. D.; Kadnikova, E. N.; Liu, J. S.; Fréchet, J. M. J. *Adv. Mater.* **2003**, *15*, 1519−1522.
(6) Prosa, T. J.; Winokur, M. J.; Moulton, J.; Smith, P.; Heeger, A. J. *Macromolecules* **1992**, *25*, 4364−4372.
(7) Meille, S. V.; Romita, V.; Caronna, T.; Lovinger, A. J.; Catellani, M.; Belobrzeckaja, L. *Macromolecules* **1997**, *30*, 7898−7905.
(8) Kline, R. J.; McGehee, M. D.; Kadnikova, E. N.; Liu, J. S.; Fréchet, J. M. J.; Toney, M. F. *Macromolecules* **2005**, *38*, 3312−3319.
(9) Kline, R. J.; Delongchamp, D. M.; Fischer, D. A.; Lin, E. K.; Richter, L. J.; Chabinyc, M. L.; Toney, M. F.; Heeney, M.; McCulloch, I. *Macromolecules* **2007**, *40*, 7960−7965.
(10) Zen, A.; Pflaum, J.; Hirschmann, S.; Zhuang, W.; Jaiser, F.; Asawapirom, U.; Rabe, J. P.; Scherf, U.; Neher, D. *Adv. Funct. Mater* **2004**, *14*, 757−764.
(11) Joshi, S.; Grigorian, S.; Pietsch, U.; Pingel, P.; Zen, A.; Neher, D.; Scherf, U. *Macromolecules* **2008**, *41*, 6800−6808.
(12) Lim, J. A.; Liu, F.; Ferdous, S.; Muthukumar, M.; Briseno, A. L. *Mater. Today* **2010**, *13*, 14−24.
(13) Mishra, A.; Ma, C.-Q.; Bäuerle, P. *Chem. Rev.* **2009**, *109*, 1141−1276.
(14) Mena-Osteritz, E.; Meyer, A.; Langeveld-Voss, B. M. W.; Janssen, R. A. J.; Meijer, E. W.; Bäuerle, P. *Angew. Chem., Int. Ed.* **2000**, *39*, 2680−2684.
(15) Bäuerle, P.; Fischer, T.; Bildlingmeier, B.; Stabel, A.; Rabe, J. *Angew. Chem. Int. Ed.* **1995**, *34*, 303−307.

(16) Takimiya, K.; Sakamoto, K.; Otsubo, T.; Kunugi, Y. *Chem. Lett.* **2006**, *35*, 492−493.

(17) Izumi, T.; Kobashi, S.; Takimiya, K.; Aso, Y.; Otsubo, T. *J. Am. Chem. Soc.* **2003**, *125*, 5286−5287.

(18) Wang, Q. L.; Qu, Y.; Tian, H. K.; Geng, Y. H.; Wang, F. S. *Macromolecules* **2011**, *44*, 1256−1260.

(19) Azumi, R.; Götz, G.; Debaerdemaeker, T.; Bäuerle, P. *Chem.— Eur. J.* **2000**, *6*, 735−744.

(20) Azumi, R.; Mena-Osteritz, E.; Boese, R.; Benet-Buchholz, J.; Bäuerle, P. *J. Mater. Chem* **2006**, *16*, 728−735.

(21) Horowitz, G.; Bachet, B.; Yassar, A.; Lang, P.; Dmanze, F.; Fave, J. L.; Gamier, F. *Chem. Mater.* **1995**, *7*, 1337−1341.

(22) *Handbook of Thiophene-Based Materials: Applications in Organic Electronics and Photonics*; Perepichka, I. F., Perepichka, D. F., Eds.; Wiley: Chichester, U.K., 2009.

(23) Chen, P.; Jäkle, F. *J. Am. Chem. Soc.* **2011**, *133*, 20142−20145.

(24) Gidron, O.; Diskin-Posner, Y.; Bendikov, M. *J. Am. Chem. Soc.* **2010**, *132*, 2148−2150.

(25) Pingel, P.; Zen, A.; Neher, D.; Lieberwirth, I.; Wenger, G.; Allard, S.; Scherf, U. *Appl. Phys. A: Mater. Sci. Process.* **2009**, *95*, 67−72.

(26) Klaerner, G.; Miller, R. D. *Macromolecules* **1998**, *31*, 2007−2009.

(27) Gierschner, J.; Cornil, J.; Egelhaaf, H.-J. *Adv. Mater.* **2007**, *19*, 173−191.

(28) Meier, H. *Angew. Chem. Int. Ed.* **2005**, *44*, 2482−2506.

(29) Bidan, G.; Nicola, A. D.; Enée, V.; Guillerez, S. *Chem. Mater.* **1998**, *10*, 1052−1058.

(30) Zhang, X.; Johnson, J. P.; Kampf, J. W.; Matzger, A. J. *Chem. Mater.* **2006**, *18*, 3470−3476.

(31) Brown, P. J.; Thomas, D. S.; Köhler, A.; Wilson, J. S.; Kim, J.-S.; Ramsdale, C. M.; Sirringhaus, H.; Friend, R. H. *Phys. Rev. B* **2003**, *67*, 064203−16.

(32) Chang, J.-F.; Clark, J.; Zhao, N.; Sirringhaus, H.; Breiby, D. W.; Andreasen, J. W.; Neilsen, M. M.; Giles, M.; Heeney, M.; McCulloch, I. *Phys. Rev. B* **2006**, *74*, 115318−12.

(33) Kohn, P.; Huettner, S.; Komber, H.; Senkovskyy, V.; Tkachov, R.; Kiriy, A.; Friend, R. H.; Steiner, U.; Huck, W. T. S.; Sommer, J.-U.; Sommer, M. *J. Am. Chem. Soc.* **2012**, *134*, 4790−4805.

(34) Ong, B. S.; Wu, Y.; Liu, P.; Gardner, S. *J. Am. Chem. Soc.* **2004**, *126*, 3378−3379.

(35) Ong, B. S.; Wu, Y.; Liu, P.; Gardner, S. *Adv. Mater.* **2005**, *128*, 4911−4916.

(36) Ko, S.; Hoke, E. T.; Pandey, L.; Hong, S.; Mondal, R.; Risko, C.; Yi, Y. P.; Noriega, R.; McGehee, M. D.; Brédas, J. −L; Salleo, A.; Bao, Z. *J. Am. Chem. Soc.* **2012**, *134*, 5222−5232.

(37) Siegrist, T.; Kloc, C.; Laudise, L. A.; Katz, H. E.; Haddon, R. C. *Adv. Mater.* **1998**, *10*, 379−382.

(38) Pan, H.; Liu, P.; Li, Y.; Wu, Y.; Ong, B. S.; Zhu, S.; Xu, G. *Adv. Mater.* **2007**, *19*, 3240−3243.

(39) Horowitz, G.; Bachet, B.; Yassar, A.; Lang, P.; Demanze, F.; Fave, J.-L.; Garnier, F. *Chem. Mater.* **1995**, *7*, 1337−1341.

(40) Mas-Torrent, M.; Rovira, C. *Chem. Rev* **2011**, *111*, 4833−4856.

(41) Fichou, D. *J. Mater. Chem* **2000**, *10*, 571−588.

(42) Curtis, M. D.; Cao, J.; Kampf, J. W. *J. Am. Chem. Soc.* **2004**, *126*, 4318−4328.

(43) Yuan, Q.; Mannsfeld, S. C. B.; Tang, M. L.; Roberts, M.; Toney, M. F.; Delongchamp, D. M.; Bao, Z. N. *Chem. Mater.* **2008**, *20*, 2763−2772.

(44) Mannsfeld, S. C. B.; Tang, M. L.; Bao, Z. N. *Adv. Mater.* **2011**, *23*, 127−131.

(45) Zhang, X. R.; Richter, L. J.; Delongchamp, D. M.; Kline, R. J.; Hammond, M. R.; McCulloch, I.; Heeney, M.; Ashraf, R. S.; Smith, J. N.; Anthopoulos, T. D.; Schroeder, B.; Geerts, Y. H.; Fischer, D. A.; Toney, M. F. *J. Am. Chem. Soc.* **2011**, *133*, 15073−15084.

(46) Yuan, Q.; Mannsfeld, S. C. B.; Tang, M. L.; Toney, M. F.; Lüning, J.; Bao, Z. N. *J. Am. Chem. Soc.* **2008**, *130*, 3502−3508.

(47) Rivnay, J.; Mannsfeld, S. C. B.; Miller, C. E.; Salleo, A.; Toney, M. F. *Chem. Rev* **2012**, *112*, 5488−5519.

(48) Jimison, L. H.; Salleo, A.; Chabinyc, M. L.; Bemstein, D. P.; Toney, M. F. *Phys. Rev. B* **2008**, *78*, 125319−18.

(49) Briseno, A. L.; Mannsfeld, S. C. B.; Lu, X.; Xiong, Y.; Jenekhe, S. A.; Bao, Z.; Xia, Y. *Nano Lett.* **2007**, *7*, 668−675.

(50) Briseno, A. L.; Mannsfeld, S. C. B.; Jenekhe, S. A.; Bao, Z.; Xia, Y. *Mater. Today* **2008**, *11*, 38−47.

(51) Kline, R. J.; McGehee, M. D.; Toney, M. F. *Nat. Mater.* **2006**, *5*, 222−228.

(52) Chang, J.-F.; Sun, B.; Breiby, D. W.; Nielsen, M. M.; Sölling, T. I.; Giles, M.; McCulloch, I.; Sirringhaus, H. *Chem. Mater.* **2004**, *16*, 4772−2776.

(53) Zen, A.; Saphiannikova, M.; Neher, D.; Grenzer, J.; Grigorian, S.; Pietsch, U.; Asawapirom, U.; Janietz, S.; Scherf, U.; Lieberwirth, I.; Wegner, G. *Macromolecules* **2006**, *39*, 2162−2171.

(54) Rivnay, J.; Steyrleuthner, R.; Jimison, L. H.; Casadei, A.; Chen, Z. H.; Toney, M. F.; Facchetti, A.; Neher, D.; Salleo, A. *Macromolecules* **2011**, *44*, 5246−5255.

(55) Rivnay, J.; Toney, M. F.; Zheng, Y.; Kauvar, I. V.; Chen, Z.; Wagner, V.; Facchetti, A.; Salleo, A. *Adv. Mater.* **2010**, *22*, 4359−4363.

(56) Rivnay, J.; Noriega, R.; Kline, R. J.; Salleo, A.; Toney, M. F. *Phys. Rev. B* **2011**, *84*, 045203−20.